Degenerate four-wave mixing as a possible source of squeezed-state light

Roy S. Bondurant
Lincoln Laboratory, Massachusetts Institute of Technology, P.O. Box 73, Lexington, Massachusetts 02173

Prem Kumar, Jeffrey H. Shapiro, and Mari Maeda
Research Laboratory of Electronics, Massachusetts Institute of Technology, Cambridge, Massachusetts 02139

(Received 14 November 1983)

The suitability of degenerate four-wave mixing (DFWM) as a source of squeezed-state (two-photon coherent state) light is investigated, both theoretically and experimentally. In previous semiclassical theory, which neglected pump quantization and loss in the nonlinear medium, Yuen and Shapiro [Opt. Lett. 4, 334 (1979)] showed that such states would be generated by 50%-50% combination of the transmitted probe (TP) and the phase-conjugate (PC) output beams of DFWM. Here the effects of quantum fluctuations in the amplitudes and phases of the pump beams are calculated in a traveling-wave finite-interaction-length DFWM configuration. It is shown that in the limit of strong pump beams and weak nonlinear coupling, the classical-pumps assumption of Yuen and Shapiro is valid. With use of this assumption, loss in the nonlinear medium is incorporated into the model by coupling the interacting modes to a set of reservoir modes. It is shown that loss presents an absolute limit on the degree of squeezing that can be achieved with DFWM. Also, for comparison with experimental work, the photoelectron statistics of the TP, PC, and 50%-50% combination modes are calculated for lossy DFWM; significant deviations are found from the predictions for lossless operation. Quantum-noise measurements on the PC and TP beams generated in sodium-vapor DFWM are described. The mixer is pumped and probed by the nearly transform-limited pulses produced by a continuous-wave-oscillator—pulse-amplifier chain dye laser at 589 nm wavelength. The normalized second-factorial moment g_2 of the PC and TP beams is determined from photoelectron-counting measurements. Inability to simultaneously achieve high DFWM reflectivity and acceptably low scattered-plus-fluorescent background, coupled with low photomultiplier quantum efficiency, restrict the experiment to a DFWM regime wherein theory predicts Poisson statistics. Experimental g_2 values corroborate this prediction, indicating that systematic and excess noises have been eliminated. No attempt was made to measure the quantum statistics of the 50%-50% combination mode.

I. INTRODUCTION

Recent work has highlighted the potential applications of two-photon coherent states (TCS), also known as squeezed states,[1] in optical communications and precision measurements.[2] These states have nonclassical noise statistics and their predicted generation schemes include the degenerate parametric amplifier (DPA), degenerate four-wave mixing (DFWM), resonance fluorescence, the free-electron laser, and two-photon and multiphoton optical bistability.[3] The preceding generation schemes have been analyzed to varying degrees of approximation, but no experimental observation of squeezed states has been reported as of yet. In this paper we present results of our theoretical and experimental investigation of the quantum statistics of light that has undergone DFWM.

Squeezed states manifest themselves in two ways that have no classical analogs. In a photon-counting measurement these states can exhibit sub-Poissonian statistics, i.e., their photon-counting variance can be smaller than their photon-counting mean. Classical light sources, on the other hand, always have count variances that equal or exceed their mean values; equality occurs for coherent-state (CS) light, which can be generated by a laser running far above threshold. For a single-mode field, such as a transform-limited pulse, sub-Poissonian statistics are equivalent to photon antibunching, i.e., the value of g_2, the normalized second-factorial moment of the modal photon-number operator,[4] being less than unity. Squeezed states can be antibunched, whereas classical states yield $g_2 \geq 1$, with equality occurring for CS light.

The second nonclassical phenomenon exhibited by these states, which can be observed via optical homodyne detection,[5] is that of quadrature-noise squeezing, hence the name squeezed state. A state is squeezed when its mean-square field fluctuation in one quadrature is less than that for a coherent state. TCS are basically minimum uncertainty squeezed states whose quadrature fluctuation product equals the limit set by the uncertainty principle, with unequal noise division between the quadratures. (In a coherent state, the uncertainty-product limit is achieved, but with equal mean-square field fluctuations in the two quadratures.) Let a be the photon annihilation operator of a fixed radiation mode of frequency ω obeying the

canonical commutation relation $[a,a^\dagger]=1$ and $a=a_1+ia_2$, $[a_1,a_2]=i/2$ for self-adjoint a_1 and a_2. In a coherent state[6] $|\alpha\rangle$, the mean-square field fluctuations are $\langle\Delta a_1^2\rangle=\langle\Delta a_2^2\rangle=\frac{1}{4}$, corresponding to a noise power spectral density $\hbar\omega/4$ for the field quadratures a_1 and a_2. For a squeezed state $|\rangle_s$, either $\langle\Delta a_1^2\rangle<\frac{1}{4}$, or $\langle\Delta a_2^2\rangle<\frac{1}{4}$ prevails. For a TCS[1] $|\beta;\mu,\nu\rangle$ with μ and ν real valued and obeying $\mu^2-\nu^2=1$, we have $\langle\Delta a_1^2\rangle=(\mu-\nu)^2/4$ and $\langle\Delta a_2^2\rangle=(\mu+\nu)^2/4$, so that $\langle\Delta a_1^2\rangle\langle\Delta a_2^2\rangle=\frac{1}{16}$. If $\mu\nu>0$, then a_1 is squeezed, and if $\mu\nu<0$, then a_2 is squeezed.

The possibility of using DFWM as a source of squeezed-state light was suggested by Yuen and Shapiro.[7] They showed that TCS should result from 50%-50% combination of the phase-conjugate (PC) reflected beam and the transmitted-probe (TP) beam. Their model, although quantum-mechanically consistent, was a simple extension of the classical description of DFWM given by Yariv and Pepper.[8] Only the PC and TP beams were treated quantum mechanically; classical descriptions of the pump beams and the medium were retained. Furthermore, other real effects that sometimes hamper DFWM experiments, such as loss and self-focusing, were ignored. Because squeezing, the key nonclassical characteristic of TCS light, is destroyed by excessive loss and fluctuations, it is desirable to include these effects in analyzing a DFWM-TCS-generation experiment. In Sec. II we extend the model of Yuen and Shapiro to include the effects of pump quantum noise and loss in the four-wave mixer. The two problems will be treated separately. It will be shown that pump quantum noise places no fundamental limits on DFWM-TCS generation, but such limits do arise from loss effects.

In Sec. III we describe an experiment we have performed to measure the quantum statistics of the PC and TP beams generated via DFWM in sodium vapor. Because DFWM occurs through the third-order nonlinearity of the mixing medium, high reflectivities require pump beams with high peak powers. Therefore, we employ a pulsed optical system and exploit the resonant enhancement of this nonlinearity. Furthermore, because a pulsed experiment does not easily lend itself to homodyne detection, we use photoelectron counting to investigate the quantum statistics, in particular the g_2 values, of the PC and TP beams. This approach has the additional benefit that g_2 values are not affected by transmission losses and low detector quantum efficiency, whereas such effects drastically curtail observations of squeezing.[9] However, photon antibunching can easily be masked (as can squeezing) by classically random excess fluctuations in the laser source or the mixing process. Accordingly, generation and detection of TCS via DFWM and photon counting requires a careful choice of operating conditions because of a variety of conflicting requirements. Indeed, our experiment was forced to operate in a DFWM regime wherein Poisson statistics ($g_2=1$) were expected theoretically. Our noise measurements corroborate this prediction, indicating that systematic and excess noises have been eliminated. We conclude in Sec. IV with a summary of our prognosis for TCS generation via DFWM in atomic vapors.

II. THEORY

A. Semiclassical model

The essence of generating squeezed states may be stated simply as follows. For a single-mode field with annihilation operator a, mix a part of this field with its phase-conjugate field represented by the creation operator $a^\dagger$ to create a new mode represented by the operator c such that

$$c=\mu a+\nu a^\dagger , \tag{1}$$

where $|\mu|^2-|\nu|^2=1$ ensures that c is an annihilation operator. Then, if the mode a is in a CS, the mode c will be in a TCS.[1] Thus, a physical process that generates a phase-conjugate field for some input field is a possible candidate for generating squeezed-state light. DFWM is such a process and was suggested by Yuen and Shapiro[7] as a possible source of squeezed states. In this section we first briefly review the theoretical model of Yuen and Shapiro to establish notation, and then extend it to include the quantum nature of the pump beams and loss incurred in the four-wave mixing medium.

We shall study the standard DFWM geometry shown in Fig. 1. Two counterpropagating pump waves intersect the object (probe) wave at a small angle in a nonlinear medium possessing a third-order ($\chi^{(3)}$) nonlinearity. All three waves are at the same frequency. A phase-matched interaction in the nonlinear medium generates a PC image wave which propagates in the opposite direction to the object wave. The outputs of the four-wave mixer are separated by means of isolators (I), and combined through an optical delay line (DL) with the proper phase relationships on a 50%-50% beam splitter (BS). As shown in Ref. 8, from a classical analysis the complex field amplitudes A_1 and A_2 of the image and object waves obey the coupled-mode equations

$$\frac{dA_1}{dz}=i\kappa^* A_2^* , \tag{2a}$$

$$\frac{dA_2}{dz}=-i\kappa^* A_1^* , \tag{2b}$$

where $\kappa^*=2^{-1}\omega\chi^{(3)}B_1B_2/cn$ gives the complex coupling

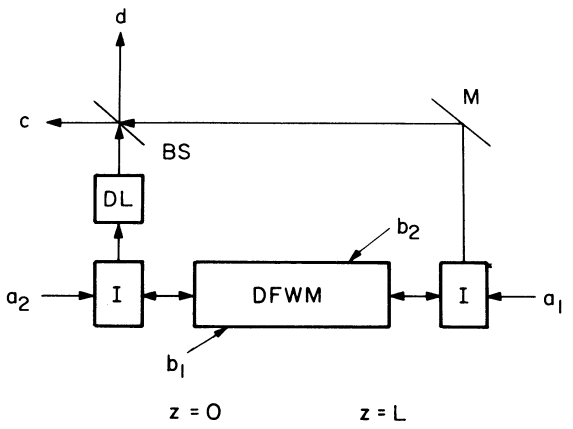

FIG. 1. Schematic for generation of TCS light via DFWM. I=isolator, DL=delay line, BS=50%-50% beam splitter, M=mirror.

constant in terms of the nondepleted pump waves of complex field amplitudes B_1 and B_2. Yuen and Shapiro[7] gave a quantum version of the above treatment assuming that the pump fields B_1 and B_2 are strong and can remain classical along with the medium described by the third-order nonlinear susceptibility $\chi^{(3)}$. They quantized the object and the image modes replacing A_j and A_j^* with the photon annihilation and creation operators a_j and $a_j^\dagger$, respectively, for $j=1,2$. Equation (2) then becomes

$$\frac{da_1}{dz}=i\kappa^* a_2^\dagger , \tag{3a}$$

$$\frac{da_2}{dz}=-i\kappa^* a_1^\dagger , \tag{3b}$$

with the following solutions:

$$a_1(0)=\mu a_1(L)-i\nu a_2^\dagger(0) , \tag{4a}$$

$$a_2(L)=\mu a_2(0)-i\nu a_1^\dagger(L) , \tag{4b}$$

where $\mu=\sec(|\kappa|L)$, $\nu=e^{-i\theta}\tan(|\kappa|L)$, $\kappa=|\kappa|e^{i\theta}$, $a_1(L)$ and $a_2(0)$ are the input fields to the four-wave mixer at $z=L$ and $z=0$, respectively.

As shown in Fig. 1, the outputs of the four-wave mixer are then combined through 50%-50% beam splitter to generate two new modes,

$$c=[a_1(0)-ia_2(L)]/2^{1/2} , \tag{5a}$$

$$d=[a_1(0)+ia_2(L)]/2^{1/2} , \tag{5b}$$

in terms of which the solutions become

$$c=\mu c_{\rm in}-\nu c_{\rm in}^\dagger , \tag{6a}$$

$$d=\mu d_{\rm in}+\nu d_{\rm in}^\dagger , \tag{6b}$$

where

$$c_{\rm in}=[a_1(L)-ia_2(0)]/2^{1/2} , \tag{7a}$$

$$d_{\rm in}=[a_1(L)+ia_2(0)]/2^{1/2} , \tag{7b}$$

are linear combinations of the input modes to the four-wave mixer. Equation (6) is of the same form as (1) and $|\mu|^2-|\nu|^2=1$, so that the modes c and d are in TCS if $a_1(L)$ and $a_2(0)$ are in CS.

The above analysis indicates that DFWM is a source of pure TCS. Depending upon the phase and magnitude of ν, arbitrary squeezing is predicted to be obtained in one of the quadratures of modes c or d. In a real experiment this is not quite so because of the assumptions made in arriving at (3). In particular, the pump modes B_1 and B_2 cannot be considered classical, and the effects of their quantum amplitude and phase fluctuations on modes c and d should be calculated. Before proceeding to do that, we note that the coupled-mode equations (3) can be derived from the following effective interaction Hamiltonian:

$$H_I=\hbar v(\kappa a_1 a_2+\kappa^* a_2^\dagger a_1^\dagger) , \tag{8}$$

where v is the speed of light in the medium. Temporal differential equations obtained from (8) in the interaction picture using

$$\frac{da_j}{dt}=-\frac{i}{\hbar}[a_j,H_I] \tag{9}$$

are converted into spatial differential equations by the change of variables $z=-vt$ for the a_1 mode and $z=vt$ for the a_2 mode.

B. Effect of quantized pumps

In this section we estimate the reduction of obtainable squeezing imposed by the quantum nature of the pump modes. Specifically, we will obtain conditions under which the pump fields may be treated as classical quantities. Our approach to this problem is somewhat different from those of recent studies. Unlike Milburn and Walls,[10] and Lugiato and Strini,[11] we do not calculate a temporal steady state for the system, because such an approach seems inappropriate for the traveling-wave finite-interaction-length geometry employed in DFWM.[12] Neither do we follow the route of Neuman and Haug,[13] and Mandel[14] to a power-series solution of the nonlinear coupled-mode equations in the limit of small parametric gain, because we are interested in operation at high gain (high conjugate reflectivity).

The complex pump field amplitudes B_1 and B_2 of Eq. (2) now become annihilation operators b_1 and b_2. The a_1 probe wave is taken to be in a CS $|\alpha_1\rangle$ on the $z=L$ plane, and the a_2 image wave is taken to be in a CS $|\alpha_2\rangle$ on the $z=0$ plane. We again assume nondepleting pump modes b_i, which remain in the coherent states $|\beta_i\rangle$ throughout the medium, with $|\beta_i|^2\gg 1+|\alpha_j|^2$ for $i,j=1,2$.

Again assuming the fields to be phase-matched plane waves, the effective interaction Hamiltonian for the modes of interest can be generalized to (classical medium described by a real third-order susceptibility)

$$\begin{aligned} H_I=\hbar v\Bigg\{ & |\bar\kappa|\Bigg[(b_1^\dagger b_2^\dagger a_1 a_2+b_1 b_2 a_1^\dagger a_2^\dagger)+\sum_{i=1}^{2} b_i^\dagger b_i a_i^\dagger a_i \\ & +2^{-1}\left[\sum_{i=1}^{2}(a_i^\dagger a_i+b_i^\dagger b_i)\right]^2\Bigg] \\ & +|\psi|\Bigg[2^{-1}\sum_{i=1}^{2}[(a_i^\dagger a_i)^2+(b_i^\dagger b_i)^2] \\ & +2\sum_{i=1}^{2} b_i^\dagger b_i a_i^\dagger a_i\Bigg]\Bigg\} . \end{aligned} \tag{10}$$

Starting from the general expression for the third-order polarization density for an isotropic medium[15]

$$\vec{\rm P}=A(\vec{\rm E}\cdot\vec{\rm E}^*)\vec{\rm E}+2^{-1}B(\vec{\rm E}\cdot\vec{\rm E})\vec{\rm E}^* , \tag{11}$$

with $|\bar\kappa|\propto A$ and $|\psi|\propto B$, the above interaction Hamiltonian can be derived from the interaction energy $(2\epsilon_0)^{-1}\int_V \vec{\rm P}\cdot\vec{\rm E}\,dV$ for the lossless classical medium by replacing the relevant field amplitudes with the corresponding operators. Equation (10) represents the general Hamiltonian obtained for typical experimental situations. In a DFWM experiment where the probe and the image waves counterpropagate, it is most convenient to exploit the polarization properties of DFWM to separate the two

beams.[16] Our choice of polarizations makes the counterpropagating pump beams orthogonally polarized so that the probe and the image beams are also orthogonally polarized, with the probe polarization being parallel to one of the pump polarizations. Similar Hamiltonians have been obtained with a different choice of beam polarizations by Marburger and Lam[17] for use in a classical analysis of DFWM with pump depletion. Terms proportional to $|\bar{\kappa}|$ are important near a one-photon transition, which is the case we will consider, and those proportional to $|\psi|$ are significant only near a two-photon transition. The first two terms in (10) lead to phase conjugation, whereas the next two are responsible for phase modulation of the beams. Since we are interested only in the phase-conjugation process, we will retain only the first two terms in the interaction Hamiltonian for our analysis of the effects of pump field quantization on quantum DFWM. Recently, the pump quantization effects due to the phase-modulation terms have been reported by Milburn, Walls, and Levenson.[18] They implicitly assumed the polarization geometry of Marburger and Lam in which it is difficult experimentally to separate the counter propagating probe and image beams. For our application the interaction Hamiltonian (10) reduces to

$$H_I=\hbar w(|\bar{\kappa}|a_1a_2b_1^{\dagger}b_2^{\dagger}+|\bar{\kappa}|b_1b_2a_1^{\dagger}a_2^{\dagger}), \tag{12}$$

which results in the following coupled-mode equations:

$$\frac{da_1}{dz}=i|\bar{\kappa}|b_1b_2a_2^{\dagger}, \tag{13a}$$

$$\frac{da_2}{dz}=-i|\bar{\kappa}|b_1b_2a_1^{\dagger}. \tag{13b}$$

These equations can be solved with the given boundary conditions to yield, writing $|\bar{\kappa}|=\bar{\kappa}$ for convenience,

$$a_1(0)=\tilde{\mu}a_1(L)-i\exp(i\tilde{\phi})\tilde{\nu}a_2^{\dagger}(0), \tag{14a}$$

$$a_2(L)=\tilde{\mu}a_2(0)-i\tilde{\nu}\exp(i\phi)a_1^{\dagger}(L). \tag{14b}$$

In Eqs. (14a) and (14b), $\tilde{\mu}=\sec[\bar{\kappa}L(\tilde{N}_1\tilde{N}_2)^{1/2}]$, $\tilde{\nu}=\tan[\bar{\kappa}L(\tilde{N}_1\tilde{N}_2)^{1/2}]$, $\exp(i\tilde{\phi})=\exp(i\tilde{\phi}_1)\exp(i\tilde{\phi}_2)$, and $\exp(i\phi)=\exp(i\phi_1)\exp(i\phi_2)$, where $\tilde{N}_j=b_jb_j^{\dagger}$, $\exp(i\tilde{\phi}_j)=b_j\tilde{N}_j^{-1/2}$, and $\exp(i\phi_j)=\tilde{N}_j^{-1/2}b_j$, for $j=1,2$.

It can be clearly seen from Eqs. (14a) and (14b) that $a_1(0)$ and $a_2(L)$ depend on both the pump amplitudes and phases. In order to assess the effects of pump quantum fluctuations and to obtain consistent expressions for $a_1(0)$ and $a_2(L)$, we use the strength of the pumps to justify replacing the operators $\tilde{\mu}$, $\tilde{\nu}$, $\exp(i\tilde{\phi})$, and $\exp(i\phi)$ with appropriately chosen classical random quantities $\tilde{\mu}$, $\tilde{\nu}$, $\tilde{\phi}$, and ϕ. The results are $\tilde{\mu}=\sec[\bar{\kappa}L(n_1n_2)^{1/2}]$, $\tilde{\nu}=\tan[\bar{\kappa}L(n_1n_2)^{1/2}]$, and $\tilde{\phi}=\phi=\Phi_1+\Phi_2$, where n_1 and n_2 are statistically independent Poisson random variables with mean values $\langle n_j\rangle=|\beta_j|^2$, and Φ_1 and Φ_2 are statistically independent Gaussian random variables with mean values[19] $\langle\Phi_j\rangle=\arg(\beta_j)\equiv\theta_j$ and variances $\langle\Delta\Phi_j^2\rangle=\frac{1}{4}|\beta_j|^{-2}$. Using these classical random variables in (14a) and (14b), we obtain for (6a) and (6b) with pump fluctuations included,

$$c=\tilde{\mu}c_{\rm in}-e^{i\phi}\tilde{\nu}c_{\rm in}^{\dagger}, \tag{15a}$$

$$d=\tilde{\mu}d_{\rm in}+e^{i\phi}\tilde{\nu}d_{\rm in}^{\dagger}, \tag{15b}$$

where the modes associated with the annihilation operators $c_{\rm in}=[a_1(L)-ia_2(0)]/2^{1/2}$ and $d_{\rm in}=[a_1(L)+ia_2(0)]/2^{1/2}$ are in the coherent states $|(\alpha_1-i\alpha_2)/2^{1/2}\rangle$ and $|(\alpha_1+i\alpha_2)/2^{1/2}\rangle$, respectively.[20]

We are now in a position to investigate the effects of amplitude and phase fluctuations on the squeezing of the TCS output modes. For simplicity, we shall examine amplitude and phase effects separately,[21] and we shall limit our presentation to the noise squeezing on the $c_1=(c+c^{\dagger})/2$ quadrature.

In the absence of pump phase fluctuations, with the mixer arranged to give $\theta_1+\theta_2=0$ and $|\beta_1|^2=|\beta_2|^2=\beta^2$, the variance of a c_1 measurement is given by

$$\langle\Delta c_1^2\rangle=\langle(\tilde{\mu}-\tilde{\nu})^2\rangle/4+\langle\Delta(\tilde{\mu}-\tilde{\nu})^2\rangle\langle c_{\rm in1}\rangle^2, \tag{16}$$

where we have used the coherent-state property $\langle\Delta c_{\rm in1}^2\rangle=\frac{1}{4}$ for $c_{\rm in1}=(c_{\rm in}+c_{\rm in}^{\dagger})/2$. The $\tilde{\mu}$ and $\tilde{\nu}$ moments needed to evaluate $\langle\Delta c_1^2\rangle$ from (16) are developed in the Appendix; with said results we obtain

$$\langle\Delta c_1^2\rangle=(\mu-\nu)^2/4+(\bar{\kappa}L\beta)^2(2\mu^2-\mu\nu)(\mu-\nu)^2/8+(\bar{\kappa}L\beta\mu)^2(\mu-\nu)^2\langle c_{\rm in1}\rangle^2/2, \tag{17}$$

where $\mu=\sec(\bar{\kappa}L\beta^2)$ and $\nu=\tan(\bar{\kappa}L\beta^2)$. The first term on the right corresponds to the classical-pump analysis of Yuen and Shapiro.[7] Equation (17) clearly shows that having intense pump beams is not sufficient to ensure they may be treated classically. Rather, in order to achieve $\langle\Delta c_1^2\rangle\approx(\mu-\nu)^2/4$ at interesting squeezing levels, we must have intense pump beams ($\beta^2\to\infty$) and weak coupling ($\bar{\kappa}L\to0$) at constant gain ($\bar{\kappa}L\beta^2$).

To evaluate the effect of phase fluctuations on the c_1-quadrature-noise squeezing we again assume $\theta_1+\theta_2=0$ and $|\beta_1|^2=|\beta_2|^2=\beta^2$. This time we suppress the amplitude fluctuations and use standard Gaussian-distribution results to obtain

$$\langle\Delta c_1^2\rangle=(\mu-\nu)^2/4+\mu\nu/8\beta^2+\nu^2\langle c_{\rm in2}\rangle^2/2\beta^2+\nu^2(\langle c_{\rm in1}\rangle^2-2\langle c_{\rm in2}\rangle^2)/8\beta^4, \tag{18}$$

where $c_{\rm in2}=(c_{\rm in}-c_{\rm in}^{\dagger})/2i$. As in the amplitude fluctuation analysis, the first term on the right is that predicted by Yuen and Shapiro,[7] and having intense pump beams does not guarantee that the extra terms may be neglected. However, $\langle\Delta c_1^2\rangle\approx(\mu-\nu)^2/4$ at interesting squeezing levels prevails with intense pump beams ($\beta^2\to\infty$) and weak coupling ($\bar{\kappa}L\to0$) at constant gain ($\bar{\kappa}L\beta^2$).

Thus, pump quantum noise does not place fundamental limits on the achievable quadrature-noise squeezing in DFWM TCS-generation experiments; our analysis demonstrates that the classical-pumps assumption is only valid when pump power becomes infinite, nonlinear coupling approaches zero, with their product remaining finite.

C. Effect of loss

Most DFWM experiments to date, and the ones reported in this paper, which achieve high PC reflectivities, ex-

ploit resonant enhancement of the $\chi^{(3)}$ nonlinearity. Operation near a resonance has the disadvantage of increasing the loss seen by the probe waves as they propagate through the medium. In this section we investigate the effect of loss on the squeezing and the photon-counting statistics of the DFWM setup shown in Fig. 1. We will assume that the pumps are noiseless classical quantities. In order to account for loss quantum mechanically we adjoin the system of Eq. (8) to two reservoirs of loss oscillators.[22] The reservoir of modes $\{b_l^1\}$ traveling in the $-z$ direction couples to the input probe wave, and the reservoir $\{b_l^2\}$ traveling in the $+z$ direction couples to the PC mode. The total Hamiltonian can therefore be written as

$$H=\sum_{s=1}^{2}\hbar\omega a_s^\dagger a_s+\hbar\sum_{s=1}^{2}\sum_{l=1}^{\infty}\omega_l b_l^{s\dagger}b_l^s +\hbar v[\kappa^*(t)a_1^\dagger a_2^\dagger+\kappa(t)a_2a_1] +\hbar\sum_{s=1}^{2}\left[a_s\sum_{l=1}^{\infty}\kappa_l^* b_l^{s\dagger}+a_s^\dagger\sum_{l=1}^{\infty}\kappa_l b_l^s\right] . \tag{19}$$

The first two terms are the free Hamiltonians for the signal and the reservoir modes. The fourth term describes the linear coupling to the loss oscillators. From Eq. (19) we obtain two coupled spatial differential equations for the slowly varying operators a_1 and a_2,

$$\frac{da_1}{dz}=\gamma a_1+i\kappa^* a_2^\dagger+G_1(z) , \tag{20a}$$

$$\frac{da_2^\dagger}{dz}=-\gamma a_2^\dagger+i\kappa a_1+G_2(z) , \tag{20b}$$

where γ is the loss per unit length and $G_1(z)$ and $G_2(z)$ are Langevin noise operators obeying

$$\gamma a_s(z)=v^{-2}\sum_l|\kappa_l|^2\int_0^z dz'\,a_s(z')\exp[i(\omega_l-\omega)(z'-z)/v], \quad s=1,2 \tag{21a}$$

$$G_1(z)=(i/v)\sum_{l=1}^{\infty}\kappa_l b_l^1(L)e^{-i(\omega-\omega_l)z/v} , \tag{21b}$$

$$G_2(z)=(i/v)\sum_{l=1}^{\infty}\kappa_l^* b_l^{2\dagger}(0)e^{-i(\omega-\omega_l)z/v} . \tag{21c}$$

These noise operators, under the Wigner-Weisskopf approximation, obey the commutation rules

$$[G_1(z),G_1^\dagger(z')]=2\gamma\delta(z-z') , \tag{22a}$$

and

$$[G_2(z),G_2^\dagger(z')]=-2\gamma\delta(z-z') . \tag{22b}$$

The set of equations (20) can be integrated subject to the appropriate boundary conditions, with the result

$$a_1(0)=Ta_1(L)-iRa_2^\dagger(0)+\Gamma_1 , \tag{23a}$$

$$a_2(L)=Ta_2(0)-iRa_1^\dagger(L)+\Gamma_2 , \tag{23b}$$

$$\Gamma_1=-T\int_0^L dz[G_1(z)F_2(L-z)+G_2(z)F_1^*(z-L)] , \tag{24a}$$

$$\Gamma_2=\int_0^L dz\,G_1^\dagger(z)[F_1^*(L-z)+iRF_2(L-z)] +\int_0^L dz\,G_2^\dagger(z)[F_2(z-L)+iRF_1(z-L)] , \tag{24b}$$

where

$$F_1(z)=i\kappa w^{-1}\sin(wz) ,$$
$$F_2(z)=\cos(wz)+\gamma w^{-1}\sin(wz) ,$$
$$w=(|\kappa|^2-\gamma^2)^{1/2} , \tag{25}$$
$$T=F_2^{-1}(L) ,$$
$$R=iF_1^*(L)/F_2(L) .$$

The constants T and R coincide with the transmission and reflection coefficients found by Abrams and Lind[23] in their analysis of the DFWM process in an absorbing medium. Indeed, our operator equations (23) reduce to their classical equations when expectation values are taken, because the noise-operator expectations $\langle\Gamma_i\rangle$ are zero. The noise operators do contribute fluctuations, which are needed to preserve the uncertainty principle. The output modes $a_1(0)$ and $a_2(L)$ satisfy the canonical commutation relations $[a_1(0),a_1^\dagger(0)]=[a_2(L),a_2^\dagger(L)]=1$ and $[a_1(0),a_2(L)]=0$, as can be verified by straightforward but tedious calculations.

We are now in a position to analyze the effects of loss on squeezing. As an example, we will evaluate $\langle\Delta c_1^2\rangle$ when $|\kappa|=\kappa$. After substituting Eqs. (23a) and (23b) into Eq. (5a) and evaluating the appropriate moments, we get

$$\langle\Delta c_1^2\rangle=\tfrac{1}{4}(T-R)^2+\frac{(T-R)^2\gamma(2N+1)}{2[w\cos(wL)-\gamma\sin(wL)]}\left[\kappa^2L-\frac{\gamma^2\sin(2wL)}{2w}-\gamma\sin^2(wL)-\frac{\kappa\gamma}{w}\sin(wL) +\kappa L[\gamma\cos(wL)+w\sin(wL)]\right] , \tag{26}$$

where N measures the initial excitation of the reservoir modes, i.e., $N=\langle b_l^{s\dagger}(0)b_l^s(0)\rangle$, and is assumed to be the same for all the modes.

Figure 2 shows a plot of the variance $\langle\Delta c_1^2\rangle$ from Eq. (26) as a function of the nonlinear coupling κL for various loss levels γL. The loss oscillators are assumed to be zero temperature with zero initial excitations. It can be seen that even a modest amount of loss, $\gamma L=0.5$, seriously reduces the amount of squeezing that is obtainable, and any initial excitation of the reservoir modes ($N\neq0$) reduces the squeezing even further, as shown in Fig. 3.

In the limit $\kappa L \gg \gamma L$, Eq. (26) reduces to

$$\langle \Delta c_1^2 \rangle \simeq (\mu-\nu)^2\{1+2\gamma L(2N+1)\sec^2(\kappa L)[1+\sin(\kappa L)]\}/4 \simeq \gamma L(2N+1)/4 \ . \tag{27}$$

So γL must be absolutely small, rather than relatively small, in order to have significant squeezing. This should be compared to the case for DPA, in which arbitrary squeezing is obtainable for any γL and N so long as κL can be made arbitrarily large compared to γL.[1] Physically, the difference seems to be because of the two counterpropagating reservoir mode ensembles, one set of modes becomes squeezed while the other becomes "expanded." In DPA there is only one reservoir ensemble, which gets squeezed the same way as the signal.

We now evaluate the effect of loss on the photon-counting statistics. In the lossless case, modes c and d of (6) are in TCS. The photon-counting distribution for a TCS is a Hermite Gaussian and has already been given by Yuen.[1] For comparison with the lossy case, we have evaluated the normalized second-factorial moment g_2 without loss for various parameter values, with the results shown in Fig. 4. The photon-counting distribution with loss becomes very complicated so we will only concentrate on g_2. Equations (23) and (5), together with the normally ordered characteristic function,[22] can be used to evaluate the following expression for g_2 (mode c):

$$g_{2,L}^{c} = (\langle -i\alpha/2^{1/2}; T,R \mid c^{\dagger 2}c^2 \mid -i\alpha/2^{1/2}; T,R \rangle + ([\mathcal{G}_2^{\dagger},\mathcal{G}_2]+[\mathcal{G}_3^{\dagger},\mathcal{G}_3]) \times \{4 \mid R \mid^2 + 2([\mathcal{G}_2^{\dagger},\mathcal{G}_2]+[\mathcal{G}_3^{\dagger},\mathcal{G}_3]) + 2 \mid T\alpha^* + R^*\alpha \mid^2\})/(\mid R \mid^2 + 2^{-1} \mid T\alpha^* + R^*\alpha \mid^2 + [\mathcal{G}_2^{\dagger},\mathcal{G}_2]+[\mathcal{G}_3^{\dagger},\mathcal{G}_3])^2 , \tag{28}$$

where $\mid -i\alpha/2^{1/2}; T,R \rangle$ is the TCS obtained in the lossless case

$$\mathcal{G}_2 = -T\int_0^L G_2(z)F_1^*(z-L)dz \ , \tag{29}$$

and

$$\mathcal{G}_3 = \int_0^L dz\, G_1^{\dagger}(z)[F_1^*(L-z)+iRF_2(L-z)]. \tag{30}$$

The rest of the functions are as defined in Eqs. (21) and (25). We have also assumed mode $a_2(0)$ in a CS $\mid \alpha \rangle$ and $a_1(L)$ in $\mid 0 \rangle$. Notice that $g_{2,L}^{c}$ is independent of the quantum efficiency of the detecting apparatus.

It can be seen from Fig. 4 (lossless case) that g_2 could be made much less than 1 at low levels of $\mid \alpha \mid^2$, i.e., the photon statistics could be made significantly sub-Poissonian. In Fig. 5, g_2 for a DFWM experiment with loss is plotted. As will be seen in the Sec. III, typical values for $\mid R \mid^2$ and T^2 in our experiment are 0.01 and 0.05, respectively, implying $\kappa L \lesssim 0.1$ and $\gamma L \gtrsim 1.5$. For these values of κL and γL, g_2 is plotted for various values of $\mid \alpha \mid^2$, the mean photon number of the input probe field. It is clear from the figure that if the region with $\mid \alpha \mid^2 \leq 10$ could be experimentally accessed, one could see a distribution which is significantly sub-Poissonian, even in the presence of moderate amounts of loss.

We therefore conclude that although pump quantum fluctuations have a negligible effect on the quantum statistics of light produced by DFWM, the presence of loss could be detrimental to the squeezing obtainable via such a process. Although the presence of loss affects the photon-counting statistics, the generation of a nonclassical state via this process could be demonstrated by measuring g_2 for the 50%-50% combination mode in a photon-counting experiment, if a suitable region of operation with $\mid \alpha \mid^2 \leq 10$ could be experimentally accessed. The results of our experimental work are presented in Sec. III.

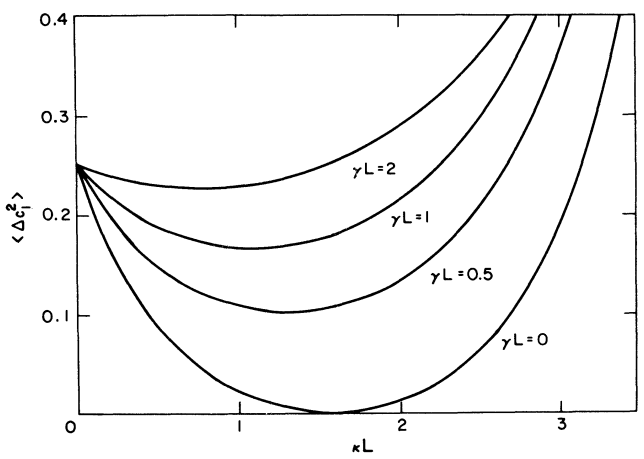

FIG. 2. Plots of the quadrature variance $\langle \Delta c_1^2 \rangle$ vs nonlinear coupling κL for various degrees of loss γL.

III. EXPERIMENT

It is clear from Eqs. (6a) and (6b) that TCS should result from the 50%-50% combination of the PC beam and the TP beam. In Sec. II C the photon-counting distribution (g_2 values in particular) for the TCS modes were presented both with and without loss in the nonlinear medium. Owing to the difficulty of making quantum-noise measurements on the output of a nonlinear optical

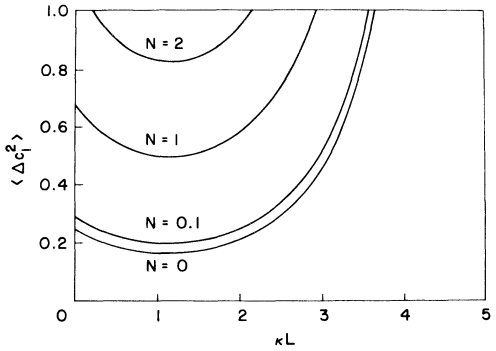

FIG. 3. Plots of the quadrature variance $\langle \Delta c_1^2 \rangle$ vs nonlinear coupling κL for various degrees of initial excitation N of the loss oscillator modes $\gamma L = 1.5$ is assumed.

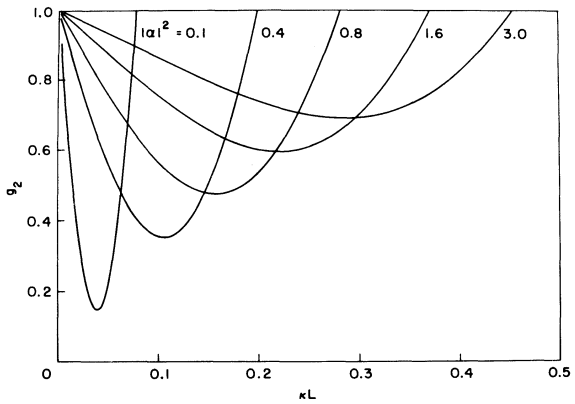

FIG. 4. Plots of the normalized second-factorial moment g_2 vs nonlinear coupling κL for various values of the average number of photons $|\alpha|^2$ in the input probe beam.

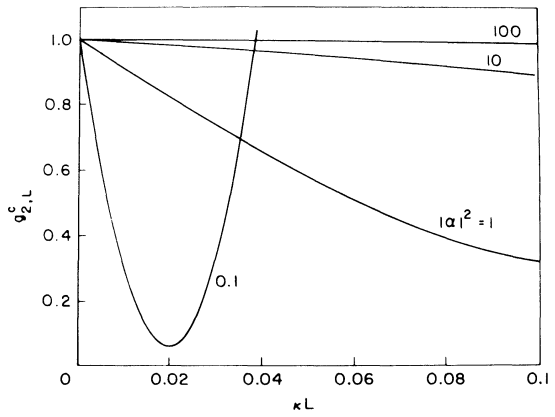

FIG. 5. Plots of the normalized second-factorial moment $g^c_{2,L}$ for lossy DFWM. $g^c_{2,L}$ is plotted for the c mode vs the nonlinear coupling κL for various values of the average number of photons $|\alpha|^2$ in the input probe beam. $\gamma L = 1.5$ is assumed.

system, we limited our initial experiment to photoelectron counting on the PC and TP beams. Therefore, it is of interest to obtain the theoretical photoelectron-counting distributions of these beams. In the absence of loss, Eqs. (4a) and (4b) can be used to obtain such distributions. The probability of detecting n primary photoelectrons is given by[22]

$$P(n)=\int \chi_A(\epsilon^{1/2}\eta^*,\epsilon^{1/2}\eta)e^{-(1-\epsilon)|\eta|^2} \times L_n(|\eta|^2)d^2\eta/\pi \ , \tag{31}$$

where ϵ is the quantum efficiency of the photodetector, $\{L_n\}$ are Laguerre polynomials, and

$$\chi_A(\eta^*,\eta)=\mathrm{tr}(\rho e^{-\eta^* a}e^{\eta a^\dagger}) \tag{32}$$

is the antinormally ordered characteristic function of the observed mode a when its density operator is ρ. Assuming the input probe wave $a_2(0)$ is in a coherent state $|\alpha\rangle$ at $z=0$ and the image wave $a_1(L)$ is in the vacuum state $|0\rangle$ at $z=L$, we find from (4a) that

$$\chi_A^{\mathrm{PC}}(\eta^*,\eta)=\exp[-|\mu\eta|^2+2i\,\mathrm{Re}(\nu\alpha^*\eta^*)] \ . \tag{33}$$

Similarly, Eq. (4b) gives

$$\chi_A^{\mathrm{TP}}(\eta^*,\eta)=\exp[-|\mu\eta|^2+2i\,\mathrm{Im}(\mu\alpha^*\eta)] \ . \tag{34}$$

Substituting into Eq. (31) we get

$$P(n)=\left\{\frac{x^n}{(1+x)^{n+1}}\right\}\exp\left\{\frac{-z|\alpha|^2}{(1+x)}\right\} \times L_n\left\{\frac{-z|\alpha|^2}{x(1+x)}\right\} , \tag{35}$$

where $x=\epsilon|\nu|^2$, $z=x$ for the PC beam, $z=\epsilon\mu^2$ for the TP beam, and $|\alpha|^2$ is the average number of photons in the coherent-state input probe beam.

Taking loss into account, Eqs. (23a) and (32) give the following characteristic function for the PC beam:

$$\chi^{\mathrm{PC}}_{A,L}(\eta^*,\eta)=\exp\{-T^2(1+[\mathcal{G}_1,\mathcal{G}_1^\dagger])|\eta|^2 +2i\,\mathrm{Re}(R\alpha^*\eta^*)\} \ , \tag{36}$$

where $\mathcal{G}_1=\int_0^L dz\,G_1(z)F_2(L-z)$, and Eqs. (21) and (25) define the rest of the quantities. A similar characteristic function is obtained for the TP beam. From Eq. (4) the normalized second-factorial moment g_2 for the lossless case is calculated to be

$$g_2^{\mathrm{PC,TP}}=1+\frac{x(x+2z|\alpha|^2)}{(x+z|\alpha|^2)^2} \ . \tag{37}$$

Note that $g_2^{\mathrm{PC,TP}}$ is independent of the quantum efficiency ϵ. In the presence of loss, the normally ordered characteristic function[22] similar to Eq. (32) can be used to obtain the following result:

$$g^{\mathrm{PC}}_{2,L}=\frac{[|R|^4(2+4|\alpha|^2+|\alpha|^4)+([\mathcal{G}_2^+,\mathcal{G}_2]\{4|R|^2(1+|\alpha|^2)+2[\mathcal{G}_2^+,\mathcal{G}_2]\})]}{(|R|^2(1+|\alpha|^2)+[\mathcal{G}_2^+,\mathcal{G}_2])^2} \ , \tag{38}$$

where, as before,

$$\mathcal{G}_2=-T\int_0^L G_2(z)F_1^*(z-L)dz \ . \tag{39}$$

Under typical experimental conditions, as we will see in the following, $\epsilon|R|^2,\epsilon|\nu|^2$, $\epsilon\mu^2\ll 1$ and $|\alpha|^2\gg 1$ prevail, so that Eqs. (35) and (37) reduce to

$$P(n)=(\epsilon|\nu|^2|\alpha|^2)^n\exp(-\epsilon|\nu|^2|\alpha|^2)/n! \tag{40}$$

for the PC beam,

$$P(n)=(\epsilon|\alpha|^2)^n\exp(-\epsilon|\alpha|^2)/n! \tag{41}$$

for the TP beam, and $g_2^{\mathrm{PC,TP}}=1$. Thus, even in the lossless case, under these conditions the distributions are Poissonian. Typical experimental conditions are such that $\gamma^2\gg\kappa^2$ and $\gamma L\simeq 1$, under which the characteristic function (36) reduces to that for a coherent state $|-iR\alpha^*\rangle$,

$[\mathcal{G}_2^{\dagger}, \mathcal{G}_2]$ in Eq. (39) approaches zero, and $g_{2,L}^{PC}$ is the same as for the lossless case.

Figure 6 shows the experimental setup. An externally stabilized cw ring dye laser (sub-MHz linewidth and less than 50-MHz/h drift) is amplified through a chain of pulsed dye-laser amplifiers pumped by the smoothed output of a Nd:YAG (yttrium aluminum garnet) laser.[24] The output pulses are 4 ns in duration with typically (10—20)% energy fluctuations and a total linewidth approximately twice the transform limit. The excess linewidth is partially correlated with the pulse-energy fluctuations due to incomplete saturation in the dye-laser amplifier chain. This is confirmed by our analysis of the fluctuations on the PC signal. The choice of such a system, as opposed to a pulsed dye-laser—oscillator-amplifier system, was dictated by the observation of strong classically random fluctuations on the PC signal at constant input pulse energy when a pulsed oscillator was employed. We will come back to the origin of these fluctuations after describing the DFWM process.

DFWM is performed in sodium vapor generated in a heat pipe oven. One to two Torr of helium is used as the buffer gas, and the inside oven temperature is maintained at 290°C implying a sodium-vapor density of 2×10^{14} atoms/cm^3. The dye laser is tuned close to the $D_2(^2S_{1/2}-{}^2P_{3/2})$ resonance transition of sodium. Under these conditions, DFWM with greater than unity reflectivity can be performed.[25] The resonantly enhanced electronic Kerr effect acts as the DFWM nonlinearity. For near-resonant excitation and short pulses the adiabatic following model[26] gives the following expression for $\chi^{(3)}$:

$$\chi^{(3)}=\pi N_a p^4/\hbar^3(\Omega-\omega)^3 , \tag{42}$$

where N_a is the atomic-number density, Ω is the transition frequency, and p is the dipole matrix element of the transition. The PC signal shows two peaks on either side of the D_2 line as the laser frequency is varied. In our experiment the higher-frequency peak was employed because the resulting spatial quality of the PC beam at our pump intensities was much better than that for the lower-frequency peak. This beam-quality difference can be ascribed to the difference in self-focusing of the signals on the two sides of the resonance line.

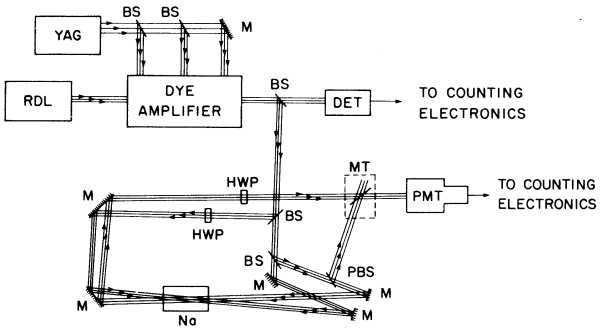

FIG. 6. Schematic of the experimental setup. RDL=ring dye laser, YAG=Nd:YAG laser with a second-harmonic generator, BS=beam splitter, M=mirror, DET=detector, PMT=photomultiplier tube, MT= mirror on a translation stage, HWP=half-wave plate, PBS=polarizing beam splitter, Na=sodium in a heat pipe oven.

The output of the dye-laser amplifier is attenuated and split in two by a 50%-50% beam splitter for use as counterpropagating pump beams of nominal intensity 1—2 kW/cm^2. A small portion of the amplifier output is further split into three parts and directed to three photodetectors. The first detector has a slow response so its output measures the energy of the dye-laser pulses for use as pulse tags during the photon-counting runs. The second detector has a fast response (50 ps risetime) and is used in conjunction with a 1-GHz-bandwidth oscilloscope to monitor the temporal quality of the pulses generated by the dye-laser system. The third detector also has a fast response; it is used in the saturation mode to trigger the photon-counting electronics. The typical triggering jitter is less than 1 ns.

A weak probe beam is derived from one of the pumps by reflection off a piece of glass. It intersects the pump beams inside the oven at a small angle, typically 1°. The mirror spacings are adjusted so that all the beams arrive in time coincidence at the center of the heat pipe oven. Polarization selection is employed to separate all of the PC beam from the counterpropagating probe beam.[16]

As mentioned earlier, there is classical randomness on the PC signal. To analyze these fluctuations several histograms such as those shown in Fig. 7 were collected. The PC signal energy and the input-probe-beam pulse energy are detected simultaneously and fed into the computer through two independent analog-to-digital convertors. After collecting 10 240 pulses, histograms are generated by defining two arrays of 2048 bins each in the computer memory and distributing the PC pulses according to their energy values in one array and the input-probe-beam pulses in the other. The histograms thus generated are

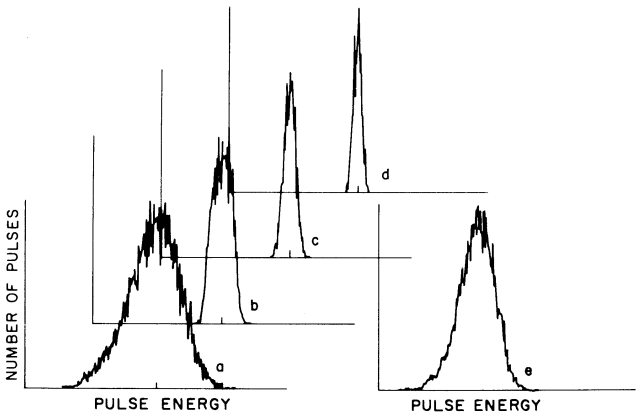

FIG. 7. Normalized pulse-energy fluctuation histograms. Horizontal scale, which is linearly proportional to the pulse energy, is the same for all the plots. The vertical scales, which are linearly proportional to the number of pulses, have been chosen to achieve common peak values. In *a*, for the PC beam, relative fluctuation level (RFL), defined as the standard deviation divided by the mean, is 0.28. In *e*, for the output of the dye-laser—oscillator-amplifier chain, RFL is 0.19. In *b*, for the PC beam when only those pulses whose input-probe-beam pulse energy falls within ±10% of the mean value are selected, RFL drops to 0.09. In *c*, same as *b* when ±5% selection is employed, RFL drops to 0.06. In *d*, RFL attains a minimum value of 0.04, even with ±1% selection.

shown in Figs. 7(a) and 7(e), respectively. Because the two pump beams are also derived from the same output of the dye-laser—oscillator-amplifier system, the width of the PC histogram is expected to be three times that of the input-pulse-energy histogram. Such is not the case because of the saturation of the $\chi^{(3)}$ nonlinearity;[27] three times as wide histograms are observed when the pump pulse energy is reduced to avoid saturation of the nonlinearity at the expense of reduced DFWM reflectivity.

When new PC-energy histograms are generated by selecting pulses falling within a specified window around the mean input-probe pulse energy, the widths of the PC histograms reduce as shown in Figs. 7(b)—7(d) indicating that most of the excess PC signal fluctuation is due to the input-pulse-energy fluctuation. In Fig. 7(d), PC pulses with input-probe pulse energies falling within 1% of the mean are selected and 4% spread of the PC energy is observed. Part of the spread (about 3%) is due to the electrical noise present in the two detectors monitoring the pulse energies.

Such a close tracking of the PC signal energy with the input pulse energy was not obtained with a pulsed oscillator-amplifier system due to fluctuations of the carrier frequency of the pulses generated by the Littman-type[28] pulsed dye laser originally used in the setup. The PC signal is sensitive to such fluctuations via the resonant denominator of Eq. (42). A detailed analysis of these fluctuations will be presented elsewhere.

The presence of these classically random fluctuations increases the g_2 value in a photon-counting experiment. If the relative energy fluctuation level is x, then the g_2 value is increased by a factor of $1+x^2$. With 4% PC-energy fluctuations, the g_2 value should be measurable with better than 0.2% accuracy. Thus pulse selection according to the input-probe pulse energy is done when the photon-counting runs are made.

To monitor these fluctuations during the course of the photon-counting runs a second probe beam is injected into the cell at the same angle to the pump beams as the first probe beam, but in a plane perpendicular to that containing the first probe beam and the pumps. The intensity of the resulting conjugate beam, called the tagging conjugate (TC), is kept high enough for the quantum fluctuations to be small, but low enough to avoid pump depletion. The TC beam is monitored by a photomultiplier tube (PMT) whose output is fed to the computer to keep track of the classical fluctuations. Several diagnostic runs were made to understand these fluctuations. The two conjugates track each other to within the noise level of the associated electronics. As with the PC beam, the TC beam also tracks the input pulse energy as monitored by the slow detector.

The photon-counting system is based on a narrow gain distribution PMT coupled to a gated (boxcar) integrator. The details and diagnostic tests of the photon-counting scheme have been described previously.[29] The beam on which photon counting is to be performed is directed into the PMT using 99.9% reflecting mirrors. All the optical components in the DFWM setup that are used in the path of the PC and TP beams are antireflection coated to minimize the reflection losses. The temporal mode is defined by the pulse duration. Pulses of a fixed energy are selected using the slow-detector tags to obtain a single mode for DFWM measurements. The systematic and random errors present in the photon-counting scheme limit the mean detected counting rate to lie between 0.2 and 0.8 counts per pulse, corresponding to 10—40 photons per pulse for our net quantum efficiency of 2% (including losses at various surfaces). Because of scattering at the windows of the heat pipe oven and fluorescence due to proximity to the D_2 resonance line of sodium, some background light is seen by the PMT. Although spatial filtering and time gating are used to minimize the background, this unwanted light ultimately dictates the operating point of the DFWM—photon-counting setup. The scattered light can be reduced below the level of the time-gated PMT dark noise by decreasing the pump intensities and increasing the angle between the probe and pump directions. However, the fluorescent emission that is spatially coherent with the PC beam persists and leads to about 0.7 counts per pulse at 1% DFWM reflectivity. The photon-counting distribution for this background is measured to be Poissonian. When the laser is tuned away from resonance by about 5 GHz, the net background is reduced to below the gated dark noise of the PMT.

The preceding considerations have forced us to perform photon counting on the PC and TP beams in the regime $\epsilon|\nu|^2 \ll 1, |\alpha|^2 \gg 1$. Under these conditions all the photon-counting distributions of interest [see Eqs. (40) and (41)] reduce to the familiar Poisson distribution for which $g_2=1$. Figure 8 shows the measured photon-counting distribution of the PC beam when the reflectivity is about 1% and a 10-dB neutral-density filter is used in front of the PMT to suppress background. (Similar data results with no attenuation at 0.1% reflectivity.) The quantity $n!P(n)$ is plotted versus n on a semi-log scale. The truncated mean and variance of this distribution are 0.520 and 0.521, respectively, giving $g_2=1.00\pm0.03$. The expected truncated g_2 for a Poisson distribution of the same truncated mean is 0.99; this Poisson distribution is shown by the straight line in Fig. 8. A mean background

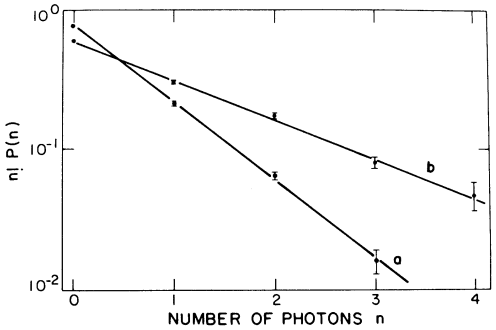

FIG. 8. Measured photon-counting distributions. The quantiy $n!P(n)$ is plotted vs n on a semi-log scale. In b, for the PC beam, the truncated mean, variance, and g_2 of the distribution are 0.520, 0.521, and 1.00 ± 0.03, respectively. The DFWM reflectivity is 1%. In a, for the TP beam, the values of the truncated mean, variance, and g_2 are 0.281, 0.282, and 1.02 ± 0.05, respectively. The DFWM reflectivity is the same as in b. The error bars on the probabilities correspond to the sampling errors in each case (Ref. 29).

count of 0.065 was present in the above run. A similar distribution is obtained for the TP beam and is also shown in Fig. 8. Thus, in accordance with the theory, no departure from the Poisson photon-counting statistics is observed. No attempt was made to measure the photon statistics of the TCS mode in light of the above experimental constraints.

IV. CONCLUSIONS

We have investigated the quantum statistics of light generated by DFWM. The quantum-mechanical fluctuations of the pump fields place no fundamental limit on obtainable squeezing, but the presence of loss in the nonlinear medium of a realistic experiment will significantly reduce the amount of squeezing available. Loss does not preclude the possibility of observing sub-Poissonian photon statistics in such a process. However, observation of such a nonclassical regime is severely limited by the practical constraints such as low quantum efficiency of the photomultiplier and high background scattering level in an atomic-vapor system. Indeed, the reason our PC and TP observations are Poissonian is our inability to simultaneously obtain high DFWM reflectivity and acceptably low background. On the basis of these results no deviation from Poisson statistics is expected in our operating regime for the 50%-50% combination mode. Moreover, to make photoelectron-counting measurements on the combination mode, interferometric stability must be maintained throughout the experimental setup over the observation interval; such stability is not critical for PC- and TP-beam measurements. Thus, no attempt was made to measure the quantum statistics of the 50%-50% combination mode. Note that it is the fluorescent background that hinders the experiment, as the scattered background can be eliminated by judicious design of the sodium cell. The fluorescent background should be studied in a fully quantum-mechanical treatment of DFWM-TCS generation, i.e., in an analysis in which the medium is also quantized.

ACKNOWLEDGMENTS

This reasearch was supported in part by the Office of Naval Research (U.S. Department of the Navy) through contracts N00014-81-K-0662 and N00014-79-C-0694. Portions of this work were presented at the Fifth Rochester Conference on Coherence and Quantum Optics, June 13–15, 1983 [see *Coherence and Quantum Optics V*, edited by L. Mandel and E. Wolf (Plenum, New York, 1983), pp. 43–50 and 767–774].

APPENDIX

To obtain Eq. (17) we must evaluate the expectations

$$\langle \sec[\bar{\kappa}L(n_1n_2)^{1/2}]\rangle ,$$

$$\langle \tan[\bar{\kappa}L(n_1n_2)^{1/2}]\rangle ,$$

$$\langle \sec^2[\bar{\kappa}L(n_1n_2)^{1/2}]\rangle ,$$

etc., where n_1 and n_2 are independent Poisson random variables with mean values $\langle n_i\rangle = |\beta_i|^2$, for $i=1,2$. Here we will outline the method for evaluating $\langle \sec[\bar{\kappa}L(n_1n_2)^{1/2}]\rangle$.

We begin with the Taylor series expansion

$$\langle \sec[\bar{\kappa}L(n_1n_2)^{1/2}]\rangle = \sum_{m=0}^{\infty} E_m(\bar{\kappa}L)^{2m}\langle n_1^m\rangle\langle n_2^m\rangle/(2m)! , \tag{A1}$$

where $\{E_m\}$ are the Euler numbers. We have that the Poisson random variable moments obey[30]

$$\langle n_i^m\rangle = \sum_{l=0}^{m} S(m,l)|\beta_i|^{2l} \approx |\beta_i|^{2m} + m(m-1)|\beta_i|^{2(m-1)}/2 , \tag{A2}$$

where $\{S(m,l)\}$ are the Stirling numbers of the second kind, and the approximate equality results when $|\beta_i|^2 \gg 1$. Substituting (A2) into (A1) we find that

$$\begin{aligned}\langle \sec[\bar{\kappa}L(n_1n_2)^{1/2}]\rangle &\approx \sec(\bar{\kappa}L|\beta_1||\beta_2|) + 2^{-1}(|\beta_1|^2+|\beta_2|^2) \\ &\quad\times \left[\frac{d^2}{dx^2}\sec(\bar{\kappa}Lx^{1/2})\right]\Bigg|_{x=|\beta_1|^2|\beta_2|^2} \\ &\approx \mu[1+(\bar{\kappa}L)^2(|\beta_1|^2+|\beta_2|^2)(\mu^2+\nu^2)/8] ,\end{aligned} \tag{A3}$$

where $\mu=\sec(\bar{\kappa}L|\beta_1||\beta_2|)$ and $\nu=\tan(\bar{\kappa}L|\beta_1||\beta_2|)$. The evaluation of expectations such as $\langle \tan[\bar{\kappa}L(n_1n_2)^{1/2}]\rangle$, $\langle \sec^2[\bar{\kappa}L(n_1n_2)^{1/2}]\rangle$, etc., may be carried out in a similar manner.

[1]For a review of the definition and properties of TCS, see H. P. Yuen, Phys. Rev. A **13**, 2226 (1976). A broader class of states, known as squeezed states, are defined as any quantum state, pure or mixed, which has less field fluctuation in a certain quadrature of the field than the coherent-state level. See H. P. Yuen, in *Coherence and Quantum Optics V*, edited by L. Mandel and E. Wolf (Plenum, New York, 1983), p. 755.

[2]H. P. Yuen and J. H. Shapiro, IEEE Trans. Inf. Theory **IT-24**, 675 (1978); **IT-26**, 78 (1980); J. H. Shapiro, H. P. Yuen, and J. A. Machado Mata, *ibid.* **IT-25**, 179 (1979); J. H. Shapiro, Opt. Lett. **5**, 351 (1980); C. M. Caves, Phys. Rev. D **23**, 1693 (1981); R. Bondurant and J. H. Shapiro, in *Coherence and Quantum Optics V*, edited by L. Mandel and E. Wolf (Plenum, New York, 1983), p. 629.

[3]G. J. Milburn and D. F. Walls, Opt. Commun. **39**, 401 (1981); L. A. Lugiato and G. Strini, *ibid.* **41**, 67 (1982); H. P. Yuen and J. H. Shapiro, Opt. Lett. **4**, 334 (1979); D. F. Walls and P. Zoller, Phys. Rev. Lett. **47**, 709 (1981); W. Becker, M. O. Scully, and M. S. Zubairy, *ibid.* **48**, 475 (1982); L. A. Lugiato and G. Strini, Opt. Commun. **41**, 374 (1982); **41**, 447 (1982); M. D. Reid and D. F. Walls, Phys. Rev. A **28**, 332 (1983).

[4]For a single-mode field $E^{(+)}(\vec{x},t)=(\hbar\omega/2\epsilon_0)^{1/2}a\phi(\vec{x},t)$,

$$g_2(\vec{x},t;\vec{x}',t')\equiv\frac{\langle E^{(-)}(\vec{x},t)E^{(-)}(\vec{x}',t')E^{(+)}(\vec{x},t)E^{(+)}(\vec{x}',t')\rangle}{\langle E^{(-)}(\vec{x},t)E^{(+)}(\vec{x},t)\rangle\langle E^{(-)}(\vec{x}',t')E^{(+)}(\vec{x}',t')\rangle}=\langle a^{\dagger 2}a^2\rangle/\langle a^\dagger a\rangle^2 , \text{ for all } \vec{x},t,\vec{x}',t' .$$

[5]H. P. Yuen and J. H. Shapiro, IEEE Trans. Inf. Theory **IT-26**, 78 (1980); H. P. Yuen and V. W. S. Chan, Opt. Lett. **8**, 177 (1983); L. Mandel, Phys. Rev. Lett. **49**, 136 (1982).

[6]R. J. Glauber, Phys. Rev. **131**, 2766 (1963); J. R. Klauder and E. C. G. Sudarshan, *Fundamentals of Quantum Optics* (Benjamin, New York, 1968).

[7]H. P. Yuen and J. H. Shapiro, Opt. Lett. **4**, 334 (1979).

[8]A. Yariv and D. M. Pepper, Opt. Lett. **1**, 16 (1977).

[9]For example, consider a mode with frequency ω and annihilation operator a that is in the TCS $|\beta;\mu,\nu\rangle$ with μ,ν positive real. We have that $\langle \Delta a_1^2 \rangle = (\mu-\nu)^2/4 < \frac{1}{4}$, where $a_1 = (a+a^\dagger)/2$. On the other hand, if we attempt to measure this squeezing via optical homodyne detection with a photodetector whose quantum efficiency η is less than one, our quadrature-noise measurement yields $\eta(\mu-\nu)^2/4+(1-\eta)/4$, as presented in Shapiro *et al.* (Ref. 2). Propagation loss can be handled in a similar fashion.

[10]G. J. Milburn and D. F. Walls, Opt. Commun. **39**, 401 (1981).

[11]L. A. Lugiato and G. Strini, Opt. Commun. **41**, 67 (1982).

[12]Our approach converts the time-dependent Heisenberg equations of motion into space-dependent coupled-mode equations subject to two-point ($z=0$, $z=L$) boundary conditions. Thus, there is no merit to a $t\rightarrow\infty$ steady state, as time has been transformed into space (via $z=\pm vt$), and only a finite length spatial interaction is involved.

[13]R. Neumann and H. Haug, Opt. Commun. **31**, 267 (1979).

[14]L. Mandel, Opt. Commun. **42**, 437 (1982).

[15]P. D. Maker and R. W. Terhune, Phys. Rev. **137**, A801 (1965).

[16]D. G. Steel, R. C. Lind, J. F. Lam, and C. R. Giuliano, Appl. Phys. Lett. **35**, 376 (1979).

[17]J. H. Marburger and J. F. Lam, Appl. Phys. Lett. **34**, 389 (1979).

[18]G. J. Milburn, D. F. Walls, and M. D. Levenson (unpublished).

[19]J. H. Shapiro and S. S. Wagner, IEEE J. Quantum Electron. (to be published).

[20]These states follow from the general treatment of the state transformations implied by unitary transformation of one set of annihilation operators into another. See Yuen and Shapiro (Ref. 2).

[21]The pump amplitude and phase fluctuations will not be treated together. Because we have converted quantum fluctuations into equivalent classical distributions, treating the latter fluctuations separately might be regarded as implying a different state for the pump radiation in each of these cases. However, our key result will be to show that for intense pump beams, weak coupling, and constant gain, the pump amplitude and phase fluctuations taken *individually* do not affect the quadrature-noise squeezing of the output modes. By the technique of iterated expectation it can be shown that in this same limit the pump amplitude and phase fluctuations taken *together* do not affect the quadrature-noise squeezing of the output modes.

[22]W. H. Louisell, *Quantum Statistical Properties of Radiation* (Wiley, New York, 1973).

[23]R. L. Abrams and R. C. Lind, Opt. Lett. **2**, 94 (1978); **3**, 205 (1978).

[24]P. Kumar and R. S. Bondurant, Appl. Opt. **22**, 1284 (1983).

[25]D. M. Bloom, P. F. Liao, and N. P. Economou, Opt. Lett. **2**, 58 (1978).

[26]D. Grischkowsky, N. S. Shiren, and R. J. Bennet, Appl. Phys. Lett. **33**, 805 (1978).

[27]D. Grischkowsky, Phys. Rev. A **7**, 2096 (1973).

[28]M. G. Littman, Opt. Lett. **3**, 138 (1978).

[29]R. S. Bondurant, P. Kumar, J. H. Shapiro, and M. M. Salour, Opt. Lett. **7**, 529 (1982).

[30]L. Comtel, *Advanced Combinatorics* (Reidel, Dordrecht, 1974).